

Synthesis, crystal structure, bovine serum albumin binding studies of 1,2,4-triazine based copper(I) complexes

Larica Pathaw^{a,1}, Themmila Khamrang^{b,1}, Arunkumar Kathiravan^{c,*},
Marappan Velusamy^{a,**}

^a Department of Chemistry, North Eastern Hill University, Shillong, 793 022, Meghalaya, India

^b C. I. College, Bishnupur, Manipur, 795126, India

^c Department of Chemistry, Vel Tech Rangarajan Dr Sagunthala R & D Institute of Science and Technology, Avadi, Chennai, 600 062, Tamil Nadu, India

ARTICLE INFO

Article history:

Received 26 December 2019

Received in revised form

28 January 2020

Accepted 29 January 2020

Available online 31 January 2020

Keywords:

Copper(I)

Crystal structure

BSA

Fluorescence

Stern–Volmer

ABSTRACT

A series of new copper complexes have been synthesized and completely characterized by pivotal analytical techniques. The coordination geometry around copper(I) complex was best described as distorted tetrahedral geometry. The binding of bovine serum albumin with Cu(I) complexes are also been investigated. The Stern–Volmer analysis on quenching data exhibits the presence of the static quenching mechanism. The binding constants were calculated using modified Stern–Volmer, Lineweaver–Burk and Scatchard plots. All the complexes exhibit the binding constants in the order of 10^4 . Thus, these results can contribute to the development of Cu(I) based drugs.

© 2020 Elsevier B.V. All rights reserved.

1. Introduction

Copper is an indispensable micronutrient encompassed in foundational life processes. The redox nature of copper makes active role in biological systems and act as a key component for many important metalloenzymes and metalloproteins [1–3]. Thus, copper has been accepted as a controlling factor for diversity of processes connected to cancer development and progression, mainly in cancer growth, angiogenesis and metastasis [4,5]. Furthermore, altered copper metabolism can also comprise a capable target for cancer therapy [6]. In this edge, quite a lot of copper complexes containing phosphanes, imidazoles, thio-semicarbazones and carbenes have been recognized as prospective anticancer agents [7–11]. Since, the commercialized drugs for cancer treatment such as cisplatin, carboplatin and metvan have shown detrimental side effects and toxicity [12]. Hence, investigation for alternative drugs has become inevitability and thus

transition metal complexes are considered. Hence, multiple copper complexes as drugs for cancer treatment were developed, which have shown excellent anticancer activities [13]. On the other hand, there is another decisive face in the development of drugs that is identification of drug–protein interactions to validate the specificity of drug action [14]. Hence, drug–protein interaction study is indeed important.

The most abundant proteins in blood are serum albumins and they play an imperative role in the transportation/deposition of many drug molecules [15]. Bovine serum albumin (BSA) has been commonly selected as the protein model due to its solubility in water/buffer [16], extraordinary binding properties [17], and resemblance to human serum albumin [18,19]. Investigations based on the binding of drugs with albumins may offer useful structural information that decides the therapeutic effect of drugs. Therefore, the studies on the binding of drugs with BSA is of crucial and great significance in chemistry, life sciences, and clinical medicine [20,21]. In this paper, in order to gain insight into the binding of metal complexes with BSA, the copper(I) complexes were considered. Since, copper is vital for the execution of different enzymes and proteins and betrothed in respiration and DNA synthesis [22]. For these motives, we are fascinated in the development of copper complexes. In this context, $[\text{Cu}(\text{L})(\text{PPh}_3)_2]\text{NO}_3$ have been

* Corresponding author.

** Corresponding author.

E-mail addresses: akathir23@gmail.com (A. Kathiravan), mvelusamy@gmail.com (M. Velusamy).

¹ Both authors are equally contributed.

synthesized and its BSA affinity properties have been investigated by UV–Vis absorbance and fluorescence spectroscopic techniques.

2. Experimental section

2.1. Materials

All the chemicals were of analytical grade and were used as received from commercial suppliers. All the solvents were distilled and degassed according to the standard procedures. Benzil, 4, 4'-dimethoxybenzil, acenaphthenequinone, phenanthrenequinone, 2-cyanopyridine, hydrazine, and analytical reagents grade chemicals and solvents were obtained commercially and used without further purification.

2.2. Methods

FT-IR spectra were recorded by KBr pellets on a PerkinElmer Spectrum FT-IR spectrometer (RX-1). ^1H NMR spectra were recorded on an FT-NMR (Bruker Avance-II 400 MHz) spectrometer by using CDCl_3 and $\text{DMSO}-d_6$ as solvents. Mass spectra were obtained on a JMS-T100LC spectrometer. UV–Visible absorption and fluorescence spectra of the samples were recorded in a Shimadzu UV-1800 spectrophotometer and Hitachi make fluorescence spectrometer (Model: F-4500), respectively. Single crystals suitable for X-ray diffraction were obtained by slow diffusion of hexane in to a solution of the complex in dichloromethane. The data collection was fulfilled using an Oxford Diffraction Xcalibur (Eos Gemini) diffractometer at ambient temperature with graphite-monochromated Mo-K α radiation ($\lambda = 0.71073 \text{ \AA}$). Data reduction and processing were carried out using the CrysAlisPro (Agilent Technologies Ltd, Yarnton, UK) suite of programmes. The structure was solved by direct methods and subsequently refined by full-matrix least squares calculations with the SHELEXL-2014 software package [23]. All non-hydrogen atoms were refined anisotropically while hydrogen atoms were placed in geometrically idealized positions and constrained to ride on their parent atoms. The graphics interface package used was PLATON, and the figures were generated using the ORTEP 3.07 generation package [24].

2.3. Synthesis of ligands

N'-aminopyridine-2-carboximidamide and metal precursor $[\text{Cu}(\text{PPh}_3)_2\text{NO}_3]$ were prepared as previously described [25,26]. The ligands 5,6-diphenyl-3-pyridin-2-yl-[1,2,4]triazine (L1), 3-pyridin-2-yl-phenanthro[9,10-e][1,2,4]triazine (L2), 9-pyridin-2-yl-7,8,10-triaza-fluoranthene (L3) and 5,6-bis-(4-methoxy-phenyl)-3-pyridin-2-yl-[1,2,4]triazine (L4) were prepared by refluxing equimolar ethanolic solutions containing the desired diketone and N'-aminopyridine-2-carboximidamide for 3 h as reported elsewhere (Scheme 1) [27].

2.4. Synthesis of complexes

The $[\text{Cu}(\text{L})(\text{PPh}_3)_2]\text{NO}_3$ complexes **1–4** were prepared by essentially following the same procedure and an illustrative example is provided below for **1** (Scheme 2). Triphenylphosphine (0.05 g, 0.2 mmol) and $[\text{Cu}(\text{PPh}_3)_2\text{NO}_3]$ (0.12 g, 0.2 mmol) were suspended in CHCl_3 (20 mL) and stirred at room temperature for 1 h. After complete dissolution of the triphenylphosphine, the corresponding N,N chelating ligand (0.08 g, 0.2 mmol) dissolved in CHCl_3 (10 mL) was added dropwise to the reaction mixture. After complete addition of the ligand, the colourless solution immediately turned yellow and then intense orange in colour and the reaction mixture was allowed to stir at room temperature overnight.

The solution was evaporated and the solid obtained was filtered off. The residue was washed with diethyl ether (40 mL) and dried under vacuum. The desired products were recrystallized from DCM:hexane (1:2) solvent mixture to give yellow to orange coloured microcrystals.

[Cu(L1)(PPh₃)₂NO₃ (1). Yellow solid; yield: 64%; ^1H NMR (400 MHz, CDCl_3) δ 8.79–8.77 (d, 1H, $J = 8 \text{ Hz}$), 8.49 (1H, s), 8.33–8.29 (m, 1H), 7.79–7.76 (m, 1H), 7.62–7.60 (d, 2H, $J = 8 \text{ Hz}$), 7.53–7.42 (m, 9H) 7.34–7.29 (m, 6H), 7.18–7.15 (m, 23H). ^{13}C NMR (400 MHz, CDCl_3) δ : 150.05, 133.16, 132.25, 130.92, 130.35, 129.97, 129.24, 129.00, 128.91, 128.88, 125.30. ^{31}P $\{^1\text{H}\}$ NMR (300 MHz, CDCl_3 , δ , ppm): 3.88. FT-IR [KBr, cm^{-1}]: 1639, 1512, 1367, 697. Anal. found (calcd) for $\text{C}_{56}\text{H}_{44}\text{CuN}_5\text{O}_3\text{P}_2$: C, 70.07 (70.03); H, 4.68 (4.62); N, 7.34 (7.29). ESI-MS (m/z): 635.10 $[\text{M}-\text{NO}_3-\text{PPh}_3]^+$.

[Cu(L2)(PPh₃)₂NO₃ (2). Dark orange solid; yield: 68%; ^1H NMR (400 MHz, CDCl_3): δ 9.35–9.33 (d, 1H, $J = 8 \text{ Hz}$), 9.20–9.18 (d, 1H, $J = 8 \text{ Hz}$), 9.02–9.00 (d, 1H, $J = 8 \text{ Hz}$), 8.67–8.62 (t, 2H, $J = 10 \text{ Hz}$), 8.55–8.54 (m, 1H) 8.43–8.40 (t, 1H, $J = 10 \text{ Hz}$), 8.02–7.98 (m, 2H) 7.93–7.86 (m, 2H) 7.82–7.79 (t, 1H, $J = 6 \text{ Hz}$), 7.32–7.27 (m, 6H), 7.19–7.15 (m, 24H). ^{13}C NMR (400 MHz, CDCl_3) δ : 149.91, 145.94, 143.52, 140.01, 134.40, 134.28, 133.15, 132.56, 132.20, 130.32, 129.20, 129.10, 128.88, 127.35, 126.51, 126.27, 125.22, 124.69, 123.75, 123.57. ^{31}P $\{^1\text{H}\}$ NMR (300 MHz, CDCl_3 , δ , ppm): 3.22. FT-IR [KBr, cm^{-1}]: 1642, 1515, 1379, 1434, 696. Anal. found (calcd) for $\text{C}_{56}\text{H}_{42}\text{CuN}_5\text{O}_3\text{P}_2$: C, 70.21 (70.18); H, 4.48 (4.42); N, 7.33 (7.31). ESI-MS (m/z): 633.18 $[\text{M}-\text{NO}_3-\text{PPh}_3]^+$.

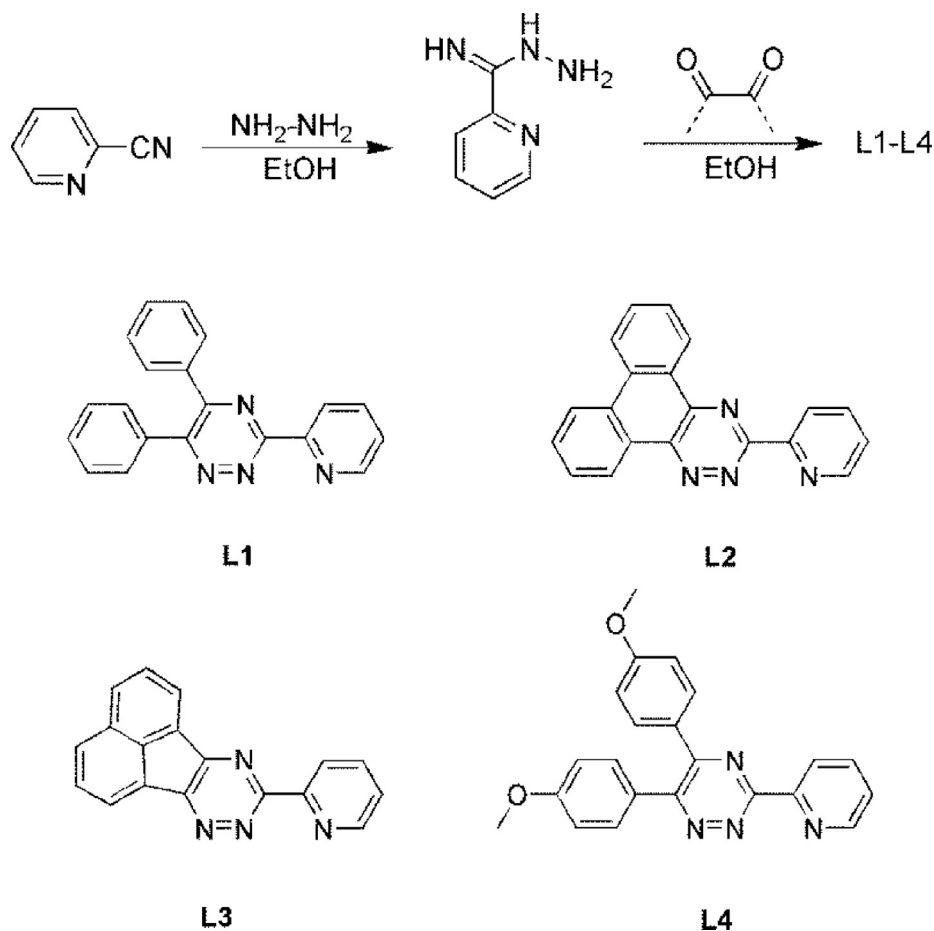
[Cu(L3)(PPh₃)₂NO₃ (3). Dark orange solid; yield: 73%; ^1H NMR (400 MHz, $\text{DMSO}-d_6$): δ 8.90–8.88 (d, 1H, $J = 8 \text{ Hz}$), 8.64–8.62 (d, 1H, $J = 8 \text{ Hz}$), 8.46–8.44 (d, 1H, $J = 8 \text{ Hz}$), 8.37–8.35 (d, 1H, $J = 8 \text{ Hz}$), 8.30–8.23 (m, 3H), 7.98–7.95 (m, 2H), 7.64–7.61 (m, 1H), 7.24 (m, 7H), 7.14 (m, 23H). ^{13}C NMR (400 MHz, CDCl_3) δ : 150.24, 149.76, 139.67, 134.16, 133.26, 132.20, 130.22, 130.03, 129.77, 129.48, 128.82, 128.41, 127.37, 127.17, 125.20, 124.64. ^{31}P $\{^1\text{H}\}$ NMR (300 MHz, CDCl_3 , δ , ppm): 3.33. FT-IR [KBr, cm^{-1}]: 1637, 1518, 1384, 1434, 695. Anal. found (calcd) for $\text{C}_{54}\text{H}_{40}\text{CuN}_5\text{O}_3\text{P}_2$: C, 69.51 (69.56); H, 4.38 (4.32); N, 7.55 (7.51). ESI-MS (m/z): 607.21 $[\text{M}-\text{NO}_3-\text{PPh}_3]^+$.

[Cu(L4)(PPh₃)₂NO₃ (4). Orange solid; yield: 69%; ^1H NMR (400 MHz, CDCl_3): δ 8.78–8.76 (d, 1H, $J = 8 \text{ Hz}$), 8.44 (m, 1H), 8.32–8.28 (t, 1H, $J = 8 \text{ Hz}$), 7.74–7.68 (m, 3H), 7.48–7.46 (d, 2H, $J = 8 \text{ Hz}$), 7.33 (m, 6H), 7.17 (m, 24H), 7.00–6.94 (m, 4H), 3.93–3.90 (d, 6H, $J = 12 \text{ Hz}$). ^{13}C NMR (400 MHz, CDCl_3) δ : 163.11, 161.74, 156.38, 156.29, 155.81, 149.83, 149.57, 139.76, 133.18, 131.92, 130.66, 130.27, 128.84, 126.48, 126.19, 125.04, 114.53, 114.42, 55.66, 55.57. ^{31}P $\{^1\text{H}\}$ NMR (300 MHz, CDCl_3 , δ , ppm): 3.00. FT-IR [KBr, cm^{-1}]: 1639, 1502, 1380, 1435, 695. Anal. found (calcd) for $\text{C}_{58}\text{H}_{48}\text{CuN}_5\text{O}_5\text{P}_2$: C, 68.31 (68.26); H, 4.81 (4.74); N, 6.81 (6.86). ESI-MS (m/z): 695.26 $[\text{M}-\text{NO}_3-\text{PPh}_3]^+$.

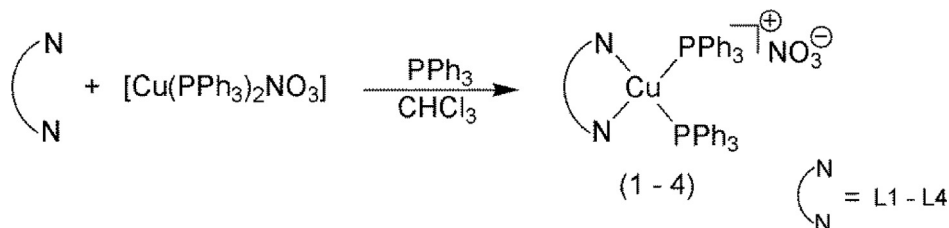
3. Results and discussion

3.1. Synthesis and characterization of copper complexes

The 3-pyridin-2-yl- [1,2,4]triazine based bidentate ligands (**L1–L4**) were synthesized by condensing pyridyl-2-amidrazone with corresponding diketone in ethanol solution. The ligands were characterized by ^1H NMR spectra. Mononuclear heteroleptic copper(I) complexes $[\text{Cu}(\text{N,N})(\text{PPh}_3)_2]\text{NO}_3$ (**1–4**) have been prepared by treating 1 equivalent of the corresponding ligand with metal precursor $[\text{Cu}(\text{PPh}_3)_2\text{NO}_3]$ in chloroform as solvent. The products were isolated as nitrate salts in good yields. The complexes have been isolated as yellow to orange coloured powders. The complexes were stable to air and non-hygroscopic in nature and were adequately soluble in acetonitrile, chloroform, dichloromethane, DMF and DMSO and insoluble in water. Based on elemental analysis, ^1H , ^{13}C NMR (Figs. S1–S8) and ESI-MS (Figs. S9–S12) the



Scheme 1. Synthesis of ligands (L1-L4).



Scheme 2. General synthesis of complexes 1-4.

complexes were formulated as $[\text{Cu}(\text{N},\text{N})(\text{PPh}_3)_2]\text{NO}_3$, and the stoichiometry of **1** is further confirmed by single crystal X-ray structure determination. The ESI-MS data reveal that the complexes retain their identity even in solution, which is supported by values of molar conductivity in DMSO ($\Delta\text{M}/\Omega^{-1} \text{ cm}^2 \text{ mol}^{-1}$: 66–72), falling in the range for 1:1 electrolytes. They are stable in the solid state as well as in solution.

The FTIR spectra of the complexes **1–4** in KBr pellets consists of characteristics peak for $\nu\text{C}=\text{C}$, $\nu\text{C}=\text{N}$ in the range of 1641–1502 cm^{-1} , the νNO_3 vibrations for nitrate anion in all the complexes falls in the range of 1367–1384 cm^{-1} . Peaks in the range of 1434–1436 cm^{-1} and 695–697 cm^{-1} in all the four complexes are assigned to the presence of triphenylphosphine similar to those Cu(I)- PPh_3 complexes [28,29]. The $^{31}\text{P}\{^1\text{H}\}$ NMR spectra (Figs. S13–S16) of the complexes **1–4** exhibited a signal corresponding to coordinated PPh_3 in the range of δ 3.0–3.88 ppm

[30,31]. The absorption spectra of Cu(I) complexes **1–4** were investigated in acetonitrile solutions, and the pertinent spectra are depicted in Fig. 1. In the absorption spectra, all the complexes exhibit intense bands in the range 370–550 nm, which probably originates from the $\pi \rightarrow \pi^*$ and $n \rightarrow \pi^*$ transitions [32,33] located in the bidentate ligands and triphenylphosphine moieties (Fig. 1). In addition, a low-energy broad absorption band is observed for all the complexes, which is characteristic of metal-to-ligand charge-transfer ($d\pi(\text{Cu}) \rightarrow \pi^*(\text{L})$ (MLCT) transitions.

3.2. Crystal structure of $[\text{Cu}(\text{L})(\text{PPh}_3)_2]\text{NO}_3$ (1)

Suitable crystals of complex **1** were obtained from the slow diffusion method. The complex crystallizes in the monoclinic space group $P2_1/c$ with unit cell parameters of $a = 13.8524(5)$, $b = 18.0692(7)$, $c = 19.8042(7)$, $\alpha = 90$, $\beta = 94.862(3)$, $\gamma = 90$ and

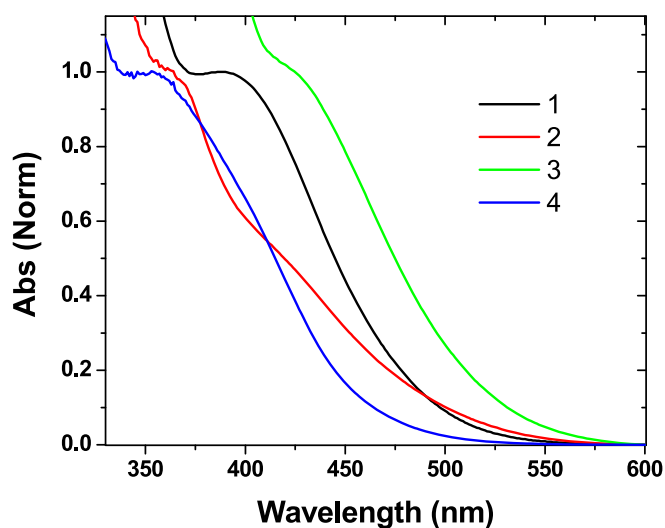


Fig. 1. Normalized absorption spectra of copper (I) complexes in acetonitrile.

$z = 4$. The molecular structure of the complex with a mono cation including the atom numbering scheme is depicted in Fig. 2. The structure refinement details and selected bond lengths and bond angles are listed in Tables 1 and 2 respectively. The asymmetric unit of complex contains a complex cation, and one nitrate as the counter ion. Copper(I) cation exhibits a distorted tetrahedral geometry by the binding of two phosphorous atoms of the PPh_3 ligand and two nitrogen atoms of the bidentate ligand. The $N1-Cu-N2$ and $P1-Cu-P2$ bond angles are $78.20(10)^\circ$, $127.91(3)^\circ$, respectively, which are far away from the ideal value of 109.5° indicating severe distortion around copper (I). The significant deviation from the ideal tetrahedral geometry is due to the restricted bite angle of the bidentate ligands. The $Cu-N_{py}$, $Cu-N_{tri}$ and $Cu-P$ distances fall within the ranges [34] expected ($Cu-N_{py} = 2.100(3)$ $Cu-P = 2.2528$ Å and $Cu-N_{tri} = 2.074(2)$ Å).

3.3. BSA-binding studies

Serum albumins are noteworthy blood proteins which have the ability to transport the drugs. Therefore, the understanding of

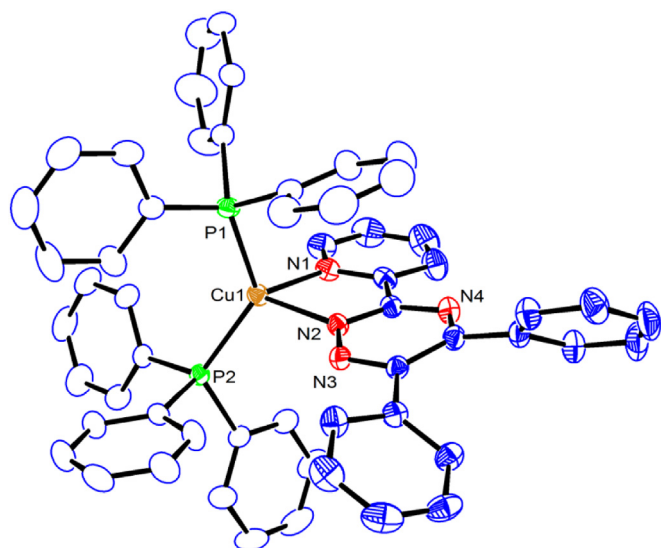


Fig. 2. ORTEP view of complex 1, showing the atom labels and 40% of the probability of ellipsoids. Anion and hydrogen atoms are omitted for clarity.

Table 1
Crystallographic data and structure refinement parameters for 1.

Formula	$C_{56}H_{44}CuN_5O_4P_2$
crystal system	Monoclinic
space group	$P2_1/c$
a (Å)	13.8524(5)
b (Å)	18.0692(7)
c (Å)	19.8042(7)
α (deg)	90
β (deg)	94.862(3)
γ (deg)	90
V (Å ³)	4939.2(3)
Z	4
μ (mm ⁻¹)	0.559
ρ_{calc} mg/mm ³	1.313
final R indices	$R_1 = 0.0499$ $wR_2 = 0.1239$
R_1^a	0.0817
wR_2^b	0.1428

$$^a R_1 = \frac{\sum |F_o| - |F_c|}{\sum |F_o|}$$

$$^b wR_2 = \frac{\sum w[(F_o^2 - F_c^2)^2]}{\sum w(F_o^2)^2}^{1/2}$$

binding strength between drug and albumin has significant research. BSA is the most widely studied protein owing to its structural homology with human serum albumin. BSA contains amino acid residues such as tryptophan, tyrosine and phenylalanine. Among the residues, tryptophan exhibits superior fluorescence intensity than other two residues [35,36]. Most importantly, the fluorescence of tryptophan is highly sensitive to the surrounding environment. Hence, the sensitive character of tryptophan is extensively utilized as endogenous fluorescent probe to understand the interaction of albumin with complexes and organic molecules. In this esteem, fluorescence quenching is an imperative method to study the interaction of drug with BSA.

A solution of BSA (5 μ M) was titrated with different concentrations of complexes (0–7 μ M) by quenching method upon excitation at 280 nm. Fig. 3 depicts the fluorescence quenching of BSA with 4. Other complexes (1–3) were also shows the similar type of quenching and spectra were shown in Figs. S17a–c. Fluorescence intensity quenching data was then evaluated according to Stern–Volmer equation (1):

$$I_0/I = 1 + K_{SV} [Q] \quad (1)$$

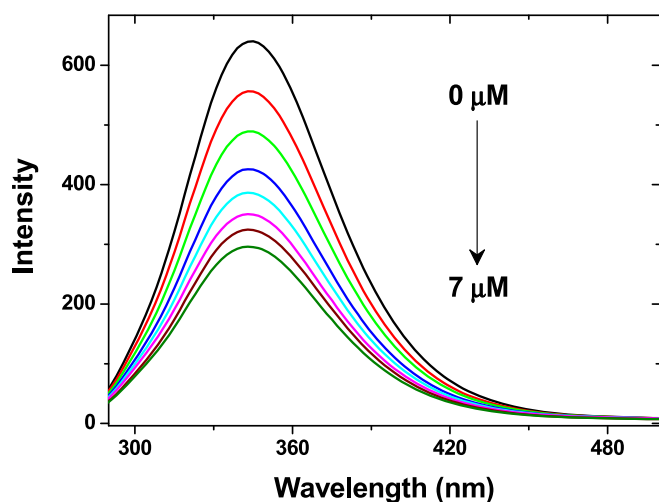
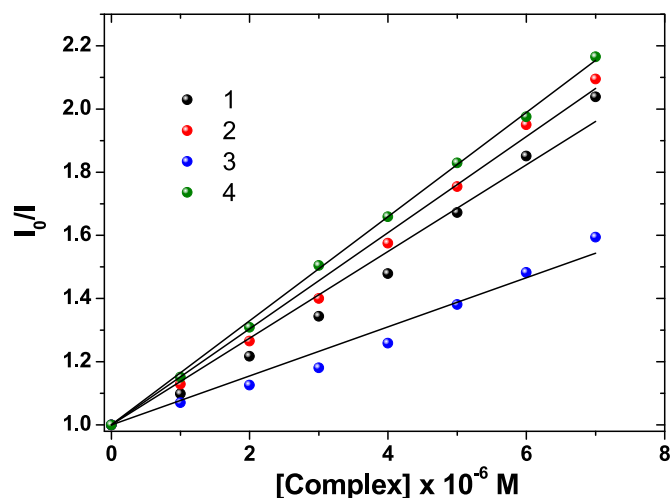
where, I_0 and I are the fluorescence intensities of BSA in the absence and presence of complexes (1–4) respectively, K_{SV} is the Stern–Volmer constant and $[Q]$ is the concentration of the complexes (1–4). Stern–Volmer plots, where the intensity ratio (I_0/I) is plotted vs. the concentration of complexes are presented in Fig. 4. As can be seen, the curves in Fig. 4 are linear which indicate the quenching may due to dynamic process. To substantiate this quenching process, the K_{SV} and k_q values were calculated from the linear regressions of the Stern–Volmer plots and are shown in Table 3. Note that, the quenching rate constant (k_q) can be calculated from K_{SV} and excited state lifetime of BSA using the following equation (2):

$$k_q = K_{SV}/\tau_0 \quad (2)$$

where, τ_0 is the fluorescence lifetime of BSA (6.05 ns) in the absence of complexes. In general, maximum collisional quenching rate constant (k_q) in water medium is $2.0 \times 10^{10} M^{-1} s^{-1}$ [37]. Obviously, the rate constant ($\sim 10^{12} M^{-1} s^{-1}$) we have calculated is greater than the limiting diffusion constant. This discrepancy in k_q supports the quenching process purely due to static.

Table 2
Selected bond lengths (Å) and angles (°) for **1**.

Bond lengths		Bond angles	
Cu1–N2	2.074(2)	N2–Cu1–N1	78.20(10)
Cu1–N1	2.100(3)	N2–Cu1–P2	111.52(7)
Cu1–P2	2.2398(8)	N1–Cu1–P2	116.43(7)
Cu1–P1	2.2658(9)	N2–Cu1–P1	102.33(7)
		N1–Cu1–P1	108.24(7)
		P2–Cu1–P1	127.91(3)

**Fig. 3.** Fluorescence spectrum of BSA with different concentrations of **4**.**Fig. 4.** Stern-Volmer plot for the quenching of BSA by complexes (**1–4**).**Table 3**
Stern–Volmer quenching constants and quenching rate constants for BSA with **1–4**.

Complexes	$K_{sv} \times 10^5 \text{ M}^{-1}$	$k_q \times 10^{13} \text{ M}^{-1} \text{ s}^{-1}$
1	1.37	2.26
2	1.52	2.51
3	0.77	1.27
4	1.64	2.71

Assuming, the quenching process is mainly static, the quenching constant or the binding constant can be evaluated from modified Stern–Volmer (MSV) equation (3) [38].

$$\frac{I_0}{\Delta I} = \frac{1}{f_a K_a} \frac{1}{Q} + \frac{1}{f_a} \quad (3)$$

where, ΔI is the difference in fluorescence intensity (i.e. $I_0 - I$) in the absence (I_0) and the presence (I) of the complexes at concentration $[Q]$, f_a is the fraction of the BSA that is initially available to complexes and K_a is the binding constant, by assuming that quenching results due to the binding of complexes with BSA. Fig. 5a shows the modified Stern–Volmer plot and the binding constants (Table 4) for all the complexes (**1–4**) have been found from the ratio of the intercept to the slope of the linear MSV plot. A good linear MSV plot again confirms that quenching mechanism between complexes and BSA belongs to the static quenching.

Further, Lineweaver–Burk analysis has been made to obtain the binding constant for the BSA-copper complexes. This analysis (equation (4)) is based on a double reciprocal plot and is somewhat similar to the MSV-equation.

$$\frac{1}{I_0 - I} = \frac{1}{I_0 K_a} \frac{1}{Q} + \frac{1}{I_0} \quad (4)$$

where, I_0 and I are the fluorescence intensities in the absence and in the presence of the complexes at concentration $[Q]$, K_a is the binding constant and is calculated from the ratio of the intercept to the slope of the straight line obtained from the Lineweaver–Burk plot. This analysis provides binding constant for BSA-complexes interaction (Fig. 5b) and the magnitude is almost same as that obtained from MSV analysis.

Lastly, Scatchard method of analysis is based on Scatchard's equation (5) has been made, from which we can calculate the binding constant and number of binding sites.

$$r/C_f = nK_a - rK_a \quad (5)$$

where r ($r = \Delta I/I_0$) is the moles of complex bound per mole of BSA, C_f is the molar concentration of the free copper complex, n is number of binding sites and K_a is the binding constant. Unlike the MSV and LWB plots, the Scatchard plot (Fig. 6) shows a negative slope as indicated by the sign in equation (5). The binding constant for BSA-complexes interaction is the slope obtained from the respective Scatchard plots. The magnitude of K_a values is comparable with that of the binding constant obtained from MSV and LWB analyses (Table 4). The number of binding sites has been calculated from the ratio of the intercept to the slope obtained from the linear plot.

4. Conclusion

We present here the preparation and characterization of a series of four $[\text{Cu}(\text{NN})(\text{PPh}_3)_2]\text{NO}_3$ complexes with sterically hindered

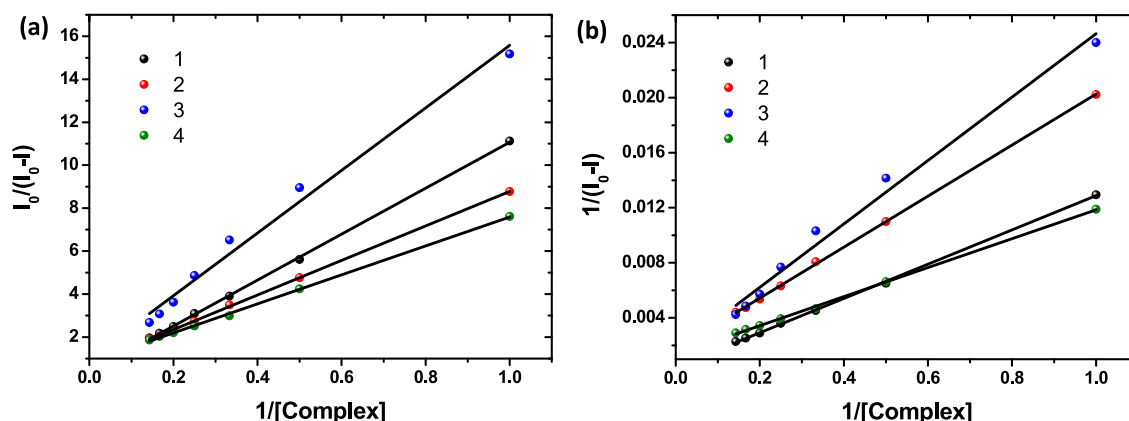


Fig. 5. Determination of binding constant from (a) modified Stern–Volmer plot and (b) Lineweaver–Burk plot.

Table 4
Binding constants and binding sites for the interaction of BSA with 1–4.

Complexes	^a K _a × 10 ⁴ M ⁻¹	^b K _a × 10 ⁴ M ⁻¹	^c K _a × 10 ⁴ M ⁻¹	n
1	3.47	3.47	7.05	1.54
2	9.32	9.33	9.05	1.36
3	6.96	6.98	1.99	1.47
4	13.36	12.63	17.31	0.97

^a from modified Stern–Volmer plot.

^b from Lineweaver–Burk plot.

^c from Scatchard plot.

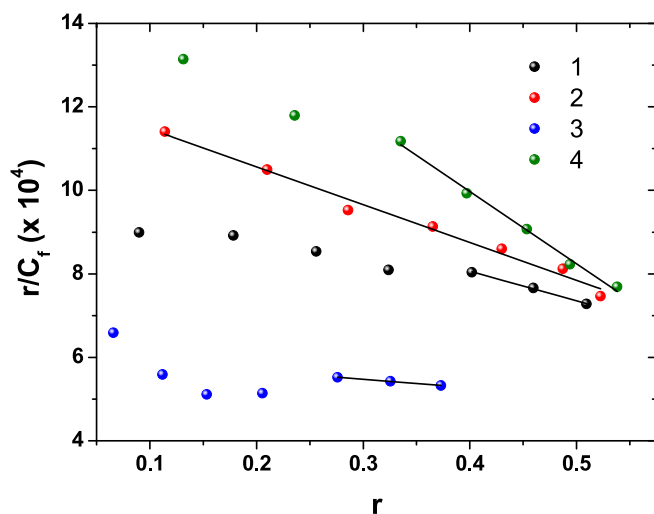


Fig. 6. Scatchard plot determining association binding constant.

triazole based chelating (N[^]N) bidentate ligand and triphenylphosphine (PPh₃). The complexes have been fully characterized by solution NMR and mass spectrometry. The single crystal structure of complex 1 confirms chelating modes for diimine and phosphine ligands and a distorted tetrahedral geometry for Cu(I). The solution absorption spectra are characterized by high energy bands arising from ligand-centered transitions. A characteristic metal to ligand [dπ(Cu) → π*(L)] MLCT band appears around 390 nm for each heteroleptic Cu(I) complexes. Serum albumin studies were carried out for all the compounds and the Stern–Volmer analysis on quenching data exhibits the presence of the static quenching mechanism. The binding constant for the interaction between

bovine serum albumin and Cu(I) complexes were calculated using modified Stern–Volmer, Lineweaver–Burk and Scatchard plots. All the complexes exhibit the binding constants in the order of 10⁴.

CRediT authorship contribution statement

Larica Pathaw: Conceptualization, Methodology, Data curation, Formal analysis, Writing - original draft. **Themmila Khamrang:** Conceptualization, Methodology, Data curation, Formal analysis. **Arunkumar Kathiravan:** Conceptualization, Methodology, Data curation, Formal analysis, Writing - original draft, Writing - review & editing. **Marappan Velusamy:** Data curation, Formal analysis, Writing - original draft, Writing - review & editing.

Acknowledgements

M.V acknowledges Science and Engineering Research Board (SERB), New Delhi EMR/2016/007955, Dated: 12. 03. 2018 for the financial support.

Appendix A. Supplementary data

Supplementary data to this article can be found online at <https://doi.org/10.1016/j.molstruc.2020.127821>.

References

- [1] K.G. Daniel, R.H. Harbach, W.C. Guida, Q.P. Dou, *Front. Biosci.* 9 (2004) 2652–2662.
- [2] D.S. Kalinowski, C. Stefani, S. Toyokuni, T. Ganz, G.J. Anderson, N.V. Subramaniam, D. Trinder, J.K. Olynyk, A. Chua, P.J. Jansson, S. Sahni, D.J. Lane, A.M. Merlot, Z. Kovacevic, M.L. Huang, C.S. Lee, D.R. Richardson, *Biochim. Biophys. Acta* 1863 (2016) 727–748.
- [3] A. Hordyjewska, L. Popiolek, J. Kocot, *Biometals.* 27 (2014) 611–621.
- [4] L.D. D'Andrea, A. Romanelli, R. Di Stasi, C. Pedone, *Dalton Trans.* 39 (2010) 7625–7636.
- [5] G. Crisponi, V.M. Nurchi, D. Fanni, C. Gerosa, S. Nemolato, G. Faa, *Coord. Chem. Rev.* 254 (2010) 876–889.
- [6] J. Wachsmann, F. Peng, *World J. Gastroenterol.* 22 (2016) 221–231.
- [7] C. Santini, M. Pellei, V. Gandin, M. Porchia, F. Tisato, C. Marzano, *Chem. Rev.* 114 (2014) 815–862.
- [8] Z. Zhang, Y. Gou, J. Wang, K. Yang, J. Qi, Z. Zhou, S. Liang, H. Liang, F. Yang, *Eur. J. Med. Chem.* 121 (2016) 399–409.
- [9] N. Mukherjee, S. Podder, S. Banerjee, S. Majumdar, D. Nandi, A.R. Chakravarty, *Eur. J. Med. Chem.* 122 (2016) 497–509.
- [10] M. Wehbe, A.W.Y. Leung, M.J. Abrams, C. Orvig, M.B. Bally, *Dalton Trans.* 46 (2017) 10758–10773.
- [11] N. Alvarez, C. Noble, M.H. Torre, E. Kremer, J. Ellena, M.P. Araujo, A.J. Costa-Filho, L.F. Mendes, M.G. Kramer, G. Facchin, *Inorg. Chim. Acta.* 466 (2017) 559–564.
- [12] Y. Jung, S.J. Lippard, *Chem. Rev.* 107 (2007) 1387–1407.
- [13] C. Santini, M. Pellei, V. Gandin, M. Porchia, F. Tisato, C. Marzano, *Chem. Rev.*

- 114 (2014) 815–862.
- [14] T. Sohrabi, M. Hosseinzadeh, S. Beigoli, M.R. Saberi, J. Chamani, J. Mol. Liq. 256 (2018) 127–138.
- [15] D.C. Carter, J.X. Ho, Adv. Protein Chem. 45 (1994) 153–203.
- [16] A. Ravindrana, A. Singha, A.M. Raichur, N. Chandrasekaran, A. Mukherjee, Colloids Surf., B 76 (2010) 32–37.
- [17] M. Idowu, E. Lamprecht, T. Nyokong, J. Photochem. Photobiol., A 198 (2008) 7–12.
- [18] Q. Wang, Y. Kuo, Y. Wang, G. Shin, C. Ruengruglikit, Q. Huang, J. Phys. Chem. B 110 (2006) 16860–16866.
- [19] P. Ju, H. Fan, T. Liu, L. Cui, S. Ai, X. Wu, Biol. Trace Elem. Res. 144 (2011) 1405–1418.
- [20] P.B. Kandagal, S. Ashoka, J. Seetharamappa, S.M.T. Shaikh, Y. Jadegoud, O.B. Ijare, J. Pharma. Biomed. 41 (2006) 393–399.
- [21] X.J. Guo, A.J. Hao, X.W. Han, P.L. Kang, Y.C. Jiang, X.J. Zhang, Mol. Biol. Rep. 38 (2011) 4185–4192.
- [22] C. Marzano, M. Pellei, F. Tisato, C. Santini, Med. Chem. 9 (2009) 185–211.
- [23] Sheldrick, G. M. SHELXTL Version 2014/7. <http://shelx.uniuc.gwdg.de/SHELX/index.php>.
- [24] L.J. Farrugia, J. Appl. Crystallogr. 45 (2012) 849–854.
- [25] C.G. Bates, P. Saejueng, J.M. Murphy, D. Venkataraman, Org. Lett. 4 (2002) 4727–4729.
- [26] E. Orselli, G.S. Kottas, A.E. Konradsson, P. Coppo, R. Fröhlich, L. De Cola, A. vanDijken, H. Börner, Inorg. Chem. 46 (2007) 11082–11093.
- [27] V. Maheshwari, D. Bhattacharyya, F.R. Fronczek, P.A. Marzilli, L.G. Marzilli, Inorg. Chem. 45 (2006) 7182–7190.
- [28] A.N. Jadhav, S.B. Pawal, S.S. Chavan, Inorg. Chim. Acta. 440 (2016) 77–83.
- [29] N. Sultana, H. Tabassum, M.S. Arayne, Indian J. Chem. A 33A (1994) 63–65.
- [30] W. Villarreal, L.C. Vegas, G. Visbal, O. Corona, R.S. Corre, J. Ellena, M.R. Cominetti, A.A. Batista, M. Navarro, Inorg. Chem. 56 (2017) 3781–3793.
- [31] L. Zhang, S. Yue, B. Li, D. Fan, Inorg. Chim. Acta. 384 (2012) 225–232.
- [32] J. Lopes, D. Alves, T.S. Morais, P.J. Costa, M.F.M. Piedade, F. Marques, M.J. Villa de Brito, M.H. Garcia, J. Inorg. Biochem. 169 (2017) 68–78.
- [33] D.A. Safin, M.P. Mitoraj, K. Robeyns, Y. Filinchuk, C.M.L.V. Velde, Dalton Trans. 44 (2015) 16824–16832.
- [34] T.S. Morais, Y. Jousseau, M.F.M. Piedade, C.R. Rodrigues, A.R. Fernandes, F. Marques, M.J. Villa de Brito, M.H. Garcia, Dalton Trans. 47 (2018) 7819–7829.
- [35] M. Skrt, E. Benedik, Č. Podlipnik, N.P. Ulrih, Food Chem. 135 (2012) 2418–2424.
- [36] P. Joshi, S. Chakraborty, S. Dey, V. Shanker, Z.A. Ansari, S.P. Singh, J. Colloid Interface Sci. 355 (2011) 402–409.
- [37] C.P. Ponce, R.P. Steer, M.F. Paige, Photochem. Photobiol. Sci. 12 (2013) 1079–1085.
- [38] S.S. Lehrer, Biochemistry 10 (1971) 3254–3263.